Contents lists available at ScienceDirect

Nuclear Engineering and Technology

journal homepage: www.elsevier.com/locate/net

Original Article

Development of a computer code for thermal–hydraulic design and analysis of helically coiled tube once-through steam generator

Yaoli Zhang [a], *, Duo Wang [a], Jianshu Lin [b], Junwei Hao [a]

[a] College of Energy, Xiamen University, 422, Siming South Road, Xiamen, Fujian 361005, China
[b] Hualong Pressurized Water Reactor Technology Corporation, Ltd., 12, Che Gong Zhuang St., Beijing, 100037, China

ARTICLE INFO

ABSTRACT

The Helically coiled tube Once-Through Steam Generator (H-OTSG) is a key piece of equipment for compact small reactors. The present study developed and verified a thermal–hydraulic design and performance analysis computer code for a countercurrent H-OTSG installed in a small pressurized water reactor. The H-OTSG is represented by one characteristic tube in the model. The secondary side of the H-OTSG is divided into single-phase liquid region, nucleate boiling region, postdryout region, and single-phase vapor region. Different heat transfer correlations and pressure drop correlations are reviewed and applied. To benchmark the developed physical models and the computer code, H-OTSGs developed in Marine Reactor X and System-integrated Modular Advanced ReacTor are simulated by the code, and the results are compared with the design data. The overall characteristics of heat transfer area, temperature distributions, and pressure drops calculated by the code showed general agreement with the published data. The thermal–hydraulic characteristics of a typical countercurrent H-OTSG are analyzed. It is demonstrated that the code can be utilized for design and performance analysis of an H-OTSG.
© 2017 Korean Nuclear Society, Published by Elsevier Korea LLC. This is an open access article under the CC BY-NC-ND license (http://creativecommons.org/licenses/by-nc-nd/4.0/).

1. Introduction

A steam generator is a type of heat exchanger specifically designed to transfer heat from a coolant to water, producing steam that can be used for power generation. Helically coiled tube steam generators (UTSGs) are widely used in the nuclear industry for their compactness, ease of manufacture, and enhanced heat transfer efficiency [1]. They are widely adopted in different nuclear power plants, such as high temperature gas-cooled reactor (HTGR), small modular reactor (SMR), Marine Reactor X (MRX), and international reactor innovative and secure (IRIS). The most prominent characteristic of flow in helically coiled tubes is the secondary flow induced by centrifugal force due to the curvature of the pipe, which results in significantly larger heat transfer and friction factors than are found for straight pipes. This allows for a design that is more compact than that of the conventional UTSG, and further makes it possible for the steam generator to be able to produce superheated steam with associated higher generation efficiency. H-OTSG is currently at the forefront of steam generator technology, with a heat transfer efficiency up to 43% higher than that of a straight tube OTSG [2]. Various mathematical models

exist to simulate UTSGs, but only limited work can be found for the new H-OTSG designs.

Hoffer et al [2] developed an H-OTSG model in RELAP5-3D by simplifying the helically coiled bundle into a single inclined tube. Steady-state results were compared with design data of modular high temperature gas-cooled reactor (MHTGR), and a loss of primary pressure transient was simulated as an exponential decrease of primary pressure. Yoon et al [3] developed a movable boundary code for H-OTSG thermal–hydraulic design that can be used for design as well as verification purposes. Tzanos [4] developed a movable boundary model for once-through steam generator analysis that is dependent on specific empirical correlations and assumes a constant pressure within heat transfer regions. Berry [5] only solved energy and continuity equations for the H-OTSG and included the pressure drop calculation for the OTSG in the overall system via an external pipe model.

Currently, small modular reactors are attracting considerable attention in China. H-OTSG is adopted in many small modular reactors, such as HTGR (INET), ACP100S china national nuclear corporation (CNNC), and ACPR50S China general nuclear power group (CGN). The thermal–hydraulic design and analysis of H-OTSG has become a common problem to be solved in all these reactors. As there is no suitable tool for the thermal–hydraulic analysis of H-OTSG in the small pressurized water reactors in China, a

---

* Corresponding author.
E-mail address: zhangyl@xmu.edu.cn (Y. Zhang).

computational code is needed to perform analysis of the steady-state and transient behavior of H-OTSG. In this study, a dedicated thermal−hydraulic analysis code for H-OTSG (THAOT) is developed. Conservation equations are applied to both primary and secondary side coolants. Empirical correlations for heat transfer coefficients and friction factors are applied. The code can be used for two purposes: to find heat transfer area for a given heat capacity for design purpose and to find the OTSG transient behavior for given geometrical design data for rating purpose. This study presents a clear picture of the development and verification of the code THAOT. The design data of H-OTSG designed in MRX as well as System-integrated Modular Advanced ReacTor (SMART) are used to benchmark the THAOT code. In addition, this paper summarizes the overall solution scheme and correlations of the THAOT, and describes code validation efforts. The transient analysis of an H-OTSG under design by THAOT will be presented in future research.

2. Mathematical models and numerical solution methods

In the THAOT code, H-OTSG is represented by one characteristic tube, as schematically shown in Fig. 1. The feedwater flows into the characteristic tube in subcooled state, absorbs heat from the primary side through a metal tube wall, and leaves the tube in superheated steam state. The primary coolant flows outside the tube in a direction opposite to that of the secondary side, and transfers heat to the secondary side through a metal tube wall. The secondary side coolant flows up inside the helically coiled tubes, whereas the primary side coolant flows across the tube bundles at a certain angle. According to the water−steam mixture state inside the tube, the secondary side is divided into four parts: subcooled section, saturated section, postdryout section, and superheated section. Subcooled boiling is neglected in the model. The high-temperature primary coolant is under high pressure and remains subcooled.
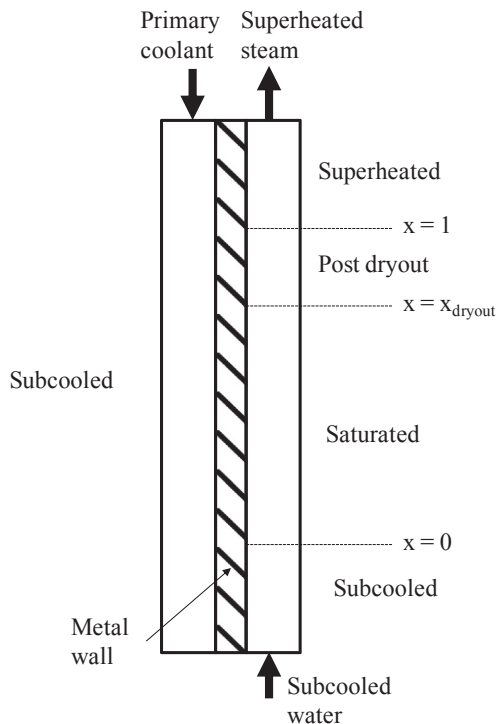

Fig. 1. Heat transfer regions in a characteristic tube.

The following assumptions are made for physical modeling of the complicated steam generator:

1. No heat conduction in the axial direction.
2. Thermal equilibrium between water and steam phases in boiling regions.
3. No reverse flow in either primary or secondary coolant.
4. Characteristic tube is divided into an arbitrary number of control volumes in axial direction, and there are homogeneous fluid properties in each control volume.
5. Effect of subcooled boiling on heat transfer and pressure drop is neglected because subcooled boiling length is small relative to the total axial wall length.

2.1. Governing equations

Conservation equations for mass, energy and momentum are used for the primary and secondary sides.

a. Mass conservation equation

$$\dot{m}_{i,\text{in}} = \dot{m}_{i,\text{out}} \tag{1}$$

b. Energy conservation equation

For the primary side:

$$c_h m_h \frac{\delta T}{\delta t} = \dot{m}_h h_{h,\text{in}} - \dot{m}_h h_{h,\text{out}} - \dot{q}_h A_h \tag{2}$$

For the secondary side:

$$c_c m_c \frac{\delta T}{\delta t} = \dot{m}_c h_{c,\text{in}} - \dot{m}_c h_{c,\text{out}} + \dot{q}_c A_c \tag{3}$$

For the metal wall, one-dimensional heat transfer equation is applied:

$$c_w m_w \frac{\delta T}{\delta t} = \dot{q}_h A_h - \dot{q}_c A_c \tag{4}$$

c. Pressure drop equation

$$\Delta P_c = \Delta P_f + \Delta P_a + \Delta P_g \tag{5}$$

Pressure drop is composed of frictional pressure drop, acceleration pressure drop, and gravitational pressure drop. In a typical H-OTSG, the coolant in the primary side flows upward, whereas the coolant in the secondary side flows downward. Therefore, the gravitational pressure drop in the primary side is negative whereas that in the secondary side is positive. Pressure drop due to form friction is neglected.

2.2. Governing equations

The heat transfer area is determined by the total transferred heat, heat transfer coefficient and log mean temperature difference. The required heat transfer area of each control volume can be calculated using the following equation:

$$\delta A_i = \frac{\delta Q_i}{K_i \times \text{LMTD}_i} \tag{6}$$

The overall heat transfer coefficient can be calculated in terms of the heat transfer coefficients on both sides of the tube wall, the thermal conductivity of the tube material, and the fouling resistance.

$$\frac{1}{K} = \frac{1}{a_1}\frac{d}{d_1} + \frac{d}{2\lambda_w}\ln\frac{d_{ex}}{d_{in}} + \frac{1}{a_2}\frac{d}{d_2} + r_{fouling} \qquad (7)$$

Heat transfer coefficients are calculated by empirical correlations, whereas the thermal conductivity of the tube material is calculated as a function of temperature. In order to benchmark the THAOT code with existing H-OTSGs, the following four types of metal material are documented in the THAOT code: Inconel-600, Inconel-690, Inconel-800, and titanium. The thermal conductivities of these materials are calculated as a function of the temperature, as follows:

$$\lambda_w^{600} = 14.262 + 0.01557 \times T \quad (W/m\,K)$$
$$\lambda_w^{690} = 11.404 + 0.01868 \times T \quad (W/m\,K)$$

$$\lambda_w^{800} = 11.666 + 0.01557 \times T \quad (W/m\,K)$$
$$\lambda_w^{Ti} = 10.174 + 0.01453 \times T \quad (W/m\,K)$$

The above thermal conductivity equations can be used within the temperature range of $20-400°C$.

2.3. Governing equations

2.3.1. Heat transfer correlations

The THAOT code includes several empirical heat transfer correlations for users to select. The default heat transfer correlations for H-OTSG are listed in Table 1. The heat transfer coefficients in helically coiled pipes are developed on the basis of straight pipe

Table 1
Heat transfer correlations in the tube side and shell side.

Correlations	Experimental parameters
Tube side [8]	
Single-phase region	$0.1 < P < 20$ MPa
$Nu = \begin{cases} 0.15Re^{0.33}Pr^{0.43}\left(\dfrac{Pr}{Pr_w}\right)^{0.25} & Re \le Re_{cr}, De \le 11.6 \\[2mm] 0.06De^{0.37}Re^{0.33}Pr^{0.43}\left(\dfrac{Pr}{Pr_w}\right)^{0.25} & Re \le Re_{cr}, De > 11.6 \\[2mm] 0.023Re^{0.8}Pr^{0.4}\left[1 + 6.3\left(1 - \dfrac{d}{D}\right)\left(\dfrac{d}{D}\right)^{1.15}\right] & Re > Re_{cr} \end{cases}$	$80 < G < 3,000$ kg/(m²s)
Critical Reynolds number [6]	$6.9 < \dfrac{D}{d} < 369$
$Re_{cr} = \begin{cases} 2300\left[1 + 210\left(\dfrac{d}{D}\right)^{1.12}\right] & \dfrac{d}{D} \le \dfrac{1}{150} \\[2mm] 12500\left(\dfrac{d}{D}\right)^{0.31} & \dfrac{1}{110} \le \dfrac{d}{D} \le \dfrac{1}{30} \\[2mm] 30000\left(\dfrac{d}{D}\right)^{0.47} & \dfrac{d}{D} \ge \dfrac{1}{24} \end{cases}$	
Nucleate boiling region	$0.1 < P < 20$ MPa
$h = h_M\sqrt{1 + 7\times10^{-9}\left(\dfrac{0.7h_0}{h_M}\right)^2\left(\dfrac{V_m\rho_f h_{fg}}{q}\right)^{\frac{3}{2}}}$	$80 < G < 3,000$ kg/(m²s)
$h_M = \sqrt{h_L^2 + (0.7h_0)^2},$	$60 < q < 800$ kW/m²
$h_f = 0.021\dfrac{\lambda_f}{d}\,Re_f^{0.85}Pr^{0.4}\left(\dfrac{d}{D}\right)^{0.1},$	$6.9 < \dfrac{D}{d} < 50$
$h_0 = 3.13q^{0.7}(0.12p^{0.14} + 1.9\times10^{-14}p^2)$	
Postdryout region	$0.1 < P < 21.5$ MPa
$Nu = \begin{cases} 0.017\theta Re_{cm}^{0.8}\,Pr_{cr}^{0.8} & \dfrac{d}{D} \ge 0.015 \\[2mm] 0.023Re_{cm}^{0.8}\,Pr_{cr}^{0.8}\left[1 - 0.1\left(\dfrac{\rho_f}{\rho_g} - 1\right)^{0.4}(1-x)^{0.4}\right] & \dfrac{d}{D} < 0.015 \end{cases}$	$100 < G < 2,000$ kg/(m²s) $0 < x < 1$
$Re_{cm} = \dfrac{Gd}{\mu_g}\left[x + \dfrac{\rho_g}{\rho_f}(1-x)\right]$	
$\theta = 1 + Y(1-x)$	
$Y = \begin{cases} 0.5\left(\dfrac{\rho_f}{\rho_g} - 1\right)^{0.8} & \dfrac{\rho_f}{\rho_g} \le 480 \\[2mm] 70 & \dfrac{\rho_f}{\rho_g} > 480 \end{cases}$	
Shell side [8]	$0.1 < P < 20$ MPa
$Nu = \begin{cases} 0.56Re^{0.5}Pr^{0.33}\left(\dfrac{Pr}{Pr_w}\right)^{0.25} & 100 < Re < 1000 \\[2mm] 0.2Re^{0.65}Pr^{0.33}\left(\dfrac{Pr}{Pr_w}\right)^{0.25} & 1000 < Re < 2\times10^5, \sigma > 2 \\[2mm] \dfrac{0.2Re^{0.65}}{\left[1 + 3\left(1 - \dfrac{\sigma}{2}\right)^3\right]^2}Pr^{0.33}\left(\dfrac{Pr}{Pr_w}\right)^{0.25} & 1000 < Re < 2\times10^5, \sigma \le 2 \\[2mm] 0.02Re^{0.84}Pr^{0.33}\left(\dfrac{Pr}{Pr_w}\right)^{0.25} & Re > 2\times10^5 \end{cases}$	

correlations with correction factors. The heat transfer coefficients in pipes are closely related to the flow patterns. Laminar and turbulent flows are the two major forms of flow in straight tubes. In helical tubes, the flow conditions are affected by the centrifugal forces that separate the liquid and gas phases due to the density difference. De is the dimensionless Dean number, which accounts for the effects of secondary flow induced by centrifugal forces in helical tubes. Transition from laminar flow to turbulent flow is governed by the critical Reynolds number Re_{cr} suggested by Cioncolini and Santini [6]. Dryout point is calculated by using the Levitan correlation [7] in the following form:

$$x = (2.7 \pm 0.3)\left(\frac{\rho_f \cdot \tau}{G^2 \cdot d_{in}}\right)^{1/4}\left(\frac{\rho_g}{\rho_f}\right)^{1/3} \qquad (8)$$

In THAOT, the constant number in the Levitan correlation is set at 2.4 for conservative consideration.

The flow patterns in the helical tubes are divided into three types considering the combined effects of Reynolds number and Dean number:

(1) When $De < 11.6$, $Re < Re_{cr}$, it is laminar flow.
(2) When $De > 11.6$, $Re < Re_{cr}$, it is laminar flow with large vortex.
(3) When $Re > Re_{cr}$, it is turbulent flow.

2.3.2. Pressure drop correlations

The pressure drop in the pipe consists of three parts: the frictional pressure drop, the gravitational pressure drop, and the acceleration pressure drop. The difference between the pressure drop in helical pipe and straight pipe lies in the frictional pressure drop. Ju et al [9] made correlations that are applied to calculate the frictional pressure drop in helical pipes, as listed in Table 2.

2.4. Overall solution method

By solving Eqs. (1–7) with additional empirical correlations for heat transfer coefficients and pressure drop calculations, THAOT can be used to determine the heat transfer area of an H-OTSG for a given heat capacity as well as to find the OTSG heat transfer capacity for a given set of geometrical design data. When THAOT is used to calculate the heat transfer area of an H-OTSG, variable time is not considered, and time-dependent equations become time-irrelevant equations. When THAOT is used to calculate heat transfer capacity, variable time is considered, and transient equations are solved. Fig. 2 shows the flow chart of the THAOT code.

3. Benchmark calculations

The THAOT code is benchmarked against the design data of two H-OTSGs. One is the steam generator of an integral reactor MRX [11,12] that was developed by Japan Atomic Energy Research Institute and Mitsubishi Heavy Industries. The other is the steam generator of SMART, developed by Korea Atomic Energy Research Institute. The results produced by THAOT are also compared with those produced using the ONCESG code developed by Korea Atomic Energy Research Institute. Although detailed design data of the H-OTSGs of MRX and SMART are different, both H-OTSGs are countercurrent-type compact steam generators. From a thermal-sizing point of view, they can be regarded as practically the same design.

3.1. Simulation of the once-through steam generator of the MRX

The MRX was developed by Japan Atomic Energy Research Institute and Mitsubishi Heavy Industries for ship propulsion. In its standard configuration, the design has a capacity of 100 MWt and
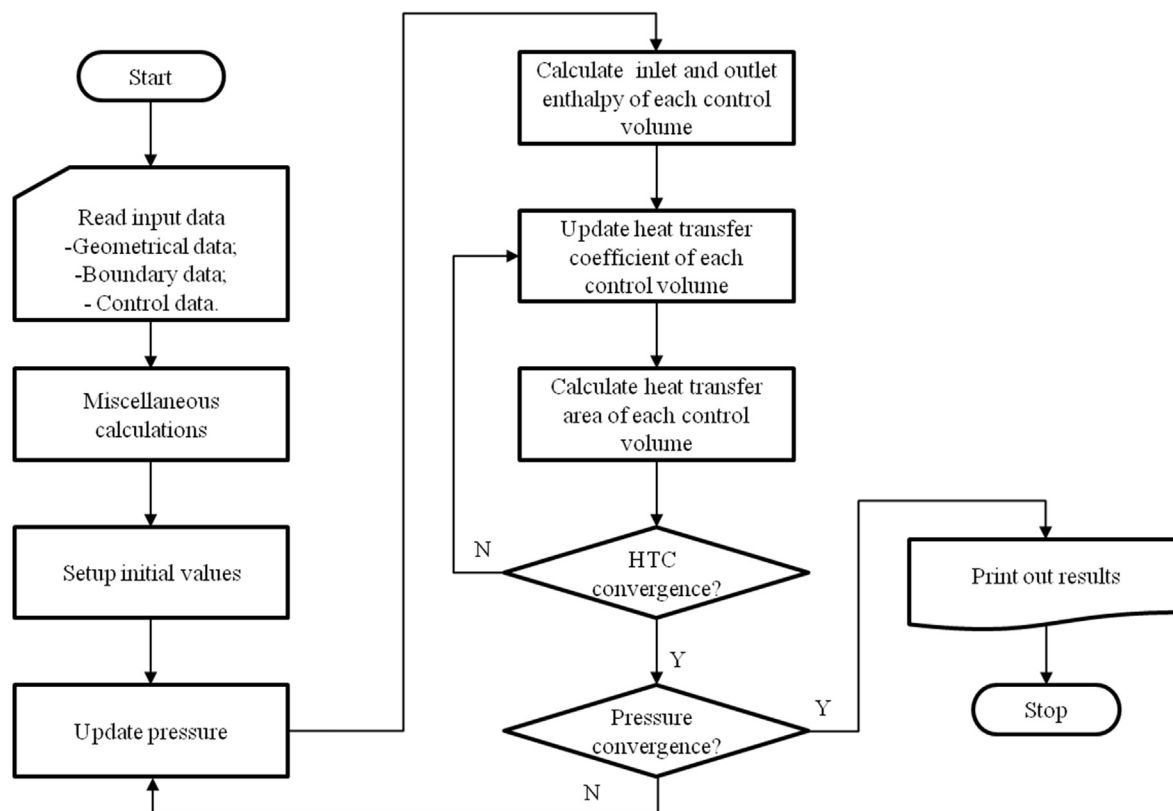
Table 2
Frictional pressure drop correlations.

Correlations	Experimental parameters
Tube side [9]	
Single-phase region	
$$\frac{f_c}{f_s} = \begin{cases} 1 & De \leq 11.6, Re \leq Re_{cr} \\ 1 + 0.015Re^{0.75}\left(\frac{d}{D}\right)^{0.4} & De > 11.6, Re \leq Re_{cr} \\ 1 + 0.11Re^{0.23}\left(\frac{d}{D}\right)^{0.14} & Re > Re_{cr} \end{cases}$$	$2.5 < P < 4.5$ MPa $200 < G < 1,500$ kg/(m^{2}s) $8.0 < \frac{D}{d} < 9.3$
when $Re \leq Re_{cr}, f_s = \frac{64}{Re}$	
when $Re > Re_{cr}, f_s = \begin{cases} \frac{0.316}{Re^{0.25}} & \text{(smooth pipe)} \\ 0.1\left(1.46\frac{\Delta}{d} + \frac{100}{Re}\right)^{0.25} & \text{(rough pipe)} \end{cases}$	
Two-phase region	$2.5 < P < 4.5$ MPa
$\Delta P_f = f\frac{L}{d}\frac{\rho_f \omega_0^2}{2}\left[1 + x\left(\frac{\rho_f}{\rho_g} - 1\right)\right]\psi$	$200 < G < 1,500$ kg/(m^{2}s)
$\psi = (1.29 + A_n x^n)\left\{1 + x\left[\left(\frac{\mu_g}{\mu_f}\right)^{0.25} - 1\right]\right\}$	$8.0 < \frac{D}{d} < 9.3$
where $A_1 = 2.19, A_2 = -3.61, A_3 = 7.35, A_4 = -5.93$	
Shell side [10]	
$\Delta P_f = 0.334 f_{eff} C_i C_n \frac{nG^2}{2\rho}$	$Pr > 0.1$
$C_i = (\cos \beta)^{-1.8}(\cos \phi)^{1.356}$	
$C_n = 1 + \frac{0.375}{n}$	
$f_{eff} \approx 1$	

Fig. 2. Flowchart of THAOT. HTC, heat transfer coefficient; N, no; THAOT, thermal−hydraulic analysis code for H-OTSG; Y, yes.

30 MWe. The steam generator of the MRX is of once-through, helically coiled tube type. The primary cooling water flows outside the tubes, whereas the secondary water and steam flow inside the tubes. The steam generator has 388 tubes arranged into 25 coil columns. Each coil column has a different number of tubes to make tubes of equal length. The design data of the MRX steam generator are listed in Table 3.

THAOT is used to calculate the heat transfer area, temperature of the coolant in the outlet of both primary side and secondary side, and pressure drop of the MRX steam generator. Different numbers of control volumes are used in the code until the results converge. 1.0×10^{-4} is set as the convergence criterion. Fouling and plugging are not taken into account. In Table 3, the results calculated by THAOT are compared with the design data of MRX and the results produced by ONCESG code. The temperature of the coolants and the heat transfer area agree well with the design data of the MRX and ONCESG results. Compared to the MRX design data, the heat transfer area is underestimated by 0.5%. The pressure drop is also underestimated compared to the MRX design data and the ONCESG results.

3.2. Simulation of the SMART once-through steam generator

SMART is a small-sized integral reactor that generates a rated thermal power of 330 MWt. It produces 100 MWe of electricity or 90 MWe of electricity and 40,000 tons of desalinated water concurrently. The capacity of SMART, shown in Table 4, is one component of the SMART steam generator. The component is of the once-through, helically coiled tube type. The primary cooling water flows outside the tubes, whereas the secondary water and steam flow inside the tubes. The primary coolant flowrate and secondary coolant flowrate in the calculation are zoomed out proportional to

the capacity. In the calculation of the SMART steam generator, design margins are taken into account, and thus the nominal SMART operating power became 339 MWt instead of the target thermal power of 330 MWt. Hence, the capacity of one component became 28.25 MWt instead of 27.5 MWt.

The results calculated by THAOT code agree well with the SMART design data and with the results calculated using the ONCESG code. Compared to the design data, the heat transfer area calculated by THAOT is overestimated by 4.4%, the pressure drop on the primary side is underestimated by 1.5%, and the pressure drop on the secondary side is overestimated by 10.0%.

3.3. Thermal−hydraulic analysis of a typical countercurrent H-OTSG

THAOT functions to analyze the thermal−hydraulic characteristics of an H-OTSG. The MRX steam generator is selected as a typical example for the analysis.

The temperature profiles of primary side coolant, secondary side coolant, and tube wall are shown in Fig. 3. The temperature of the primary coolant decreases gently along the flow direction when transferring heat to the secondary side. The temperature of the secondary side rises to the saturated temperature and then decreases slightly because of pressure drop; temperature finally rises again when the water becomes superheated vapor. The temperature of the tube wall varies because of different heat transfer coefficients in different tube positions. There is an abrupt temperature rise in the tube wall in the position where the tube length is about 29 m; the reason for this is that water dries out at this position (see Fig. 4); heat transfer coefficient varies sharply and causes an abrupt temperature rise.

Table 3
MRX design data and calculation results.

Input conditions and output results	MRX [3,12]	ONCESG results [3]	THAOT results
Input			
Capacity		100 MWt	
Total no. of tubes		388	
Tube material		Inconel-800	
Tube inner/outer diameter		14.8/19 mm	
No. of coils		25	
Radial pitch		25 mm	
Axial pitch		25 mm	
Innermost coil diameter		2.095 m	
Outermost coil diameter		3.295 m	
Primary coolant flowrate		1,250 kg/s	
Secondary coolant flowrate		46.67 kg/s	
P_{hot}		12 MPa	
T_{hot}		297.5°C	
P_{steam}		4 MPa	
$P_{feedwater}$		185°C	
Output			
T_{cold} (°C)	282.5	282.5	282.5
T_{steam} (°C)	289	289	289
Heat transfer area (m^2, inside)	754	672.5–728.1	750.0
Axial height (m)	2.1	1.71–1.85	2.09
Average tube length (m)	—	37.3–40.4	41.6
Shell-side pressure drop (MPa)	9.0×10^{-3}	1.2×10^{-2}	4.2×10^{-3}
Tube-side pressure drop (MPa)	0.64	0.45–0.49	0.42

MRX, Marine Reactor X; THAOT, thermal–hydraulic analysis code for H-OTSG.

Fig. 5 shows the velocity variation of the coolants on the primary and secondary sides along the tube. The velocity of the primary side coolant remains almost the same, whereas the velocity of the secondary side coolant rises from less than 1 m/s to 40 m/s owing to phase change. Furthermore, the velocity of the secondary side coolant does not increase linearly. The reason for this is that the velocity rise is largely affected by the heat transfer coefficient on the secondary side. As illustrated in Fig. 6, the heat transfer coefficient of the primary side remains almost constant. When the heat

transfer coefficient increases in the saturated boiling region, the velocity of the secondary side coolant rises quickly. The heat transfer coefficient decreases in the postdryout region, and the slope of the velocity of the secondary side decreases.

Fig. 7 shows the heat resistance profiles of the MRX steam generator. The heat resistance of the primary side is relatively small; the heat resistance of the wall is the dominant heat resistance in 70% of the steam generator, and the heat resistance of the secondary side becomes the dominant heat resistance after dryout. If we want to make improvements to the H-OTSG to make it more compact, the most effective way would be to enhance the tube wall material.

The dryout point starts when the humidity exceeds 0.89. According to the Levitan correlation [see Eq. (8)], when the constant number in the equation varies from 2.4 to 3.0, the humidity of the dryout point varies from 0.89 to 1.0. As heat resistance is much larger in the postdryout region than it is in the two-phase region, a conservative result is applied in the THAOT code for the purpose of design and analysis.

Table 4
SMART Design data and calculation results.

Input conditions and output results	SMART [3]	ONCESG results [3]	THAOT results
Input			
Capacity		28.25 MWt	
Total no. of tubes		324	
Tube material		Titanium	
Tube inner/outer diameter		9/12 mm	
No. of coils		17	
Radial pitch		17 mm	
Axial pitch		13.5 mm	
Innermost coil diameter		0.182 m	
Outermost coil diameter		0.726 m	
Primary coolant flowrate		128.3 kg/s	
Secondary coolant flowrate		12.7 kg/s	
P_{hot}		15 MPa	
T_{hot}		310°C	
P_{steam}		3.4 MPa	
$P_{feedwater}$		180°C	
Output			
T_{cold} (°C)	268.5	268.3	268.4
T_{steam} (°C)	300	300.9	300.1
Heat transfer area (m^2, middle)	168.8	161.3–172.4	176.3
Axial height (m)	2.8	2.67–2.86	2.92
Average tube length (m)	15.8	15.1–16.1	16.5
Shell-side pressure drop (MPa)	2.57×10^{-3}	3.5×10^{-3}	2.53×10^{-3}
Tube-side pressure drop (MPa)	0.3	0.34–0.35	0.33

SMART, System-integrated Modular Advanced ReacTor; THAOT, thermal-hydraulic analysis code for H-OTSG.
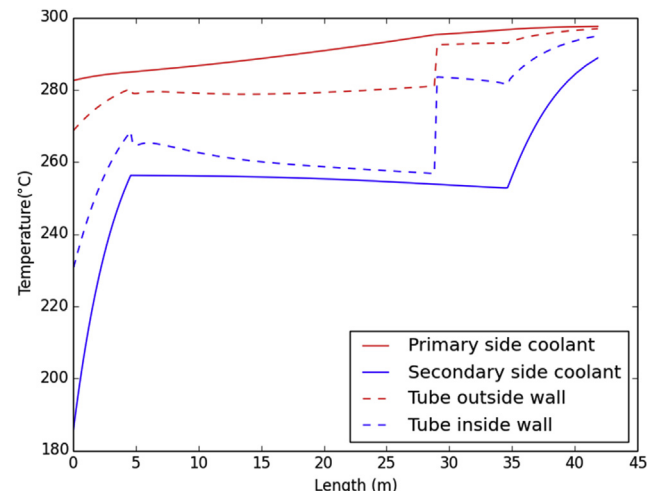
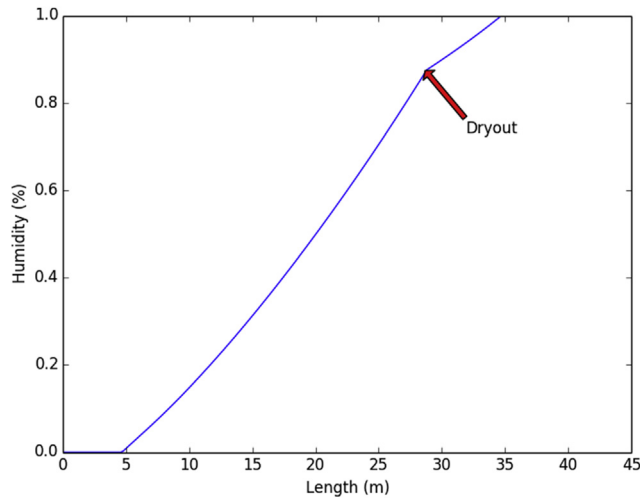**Fig. 3.** Temperature profiles in the MRX steam generator. MRX, Marine Reactor X.

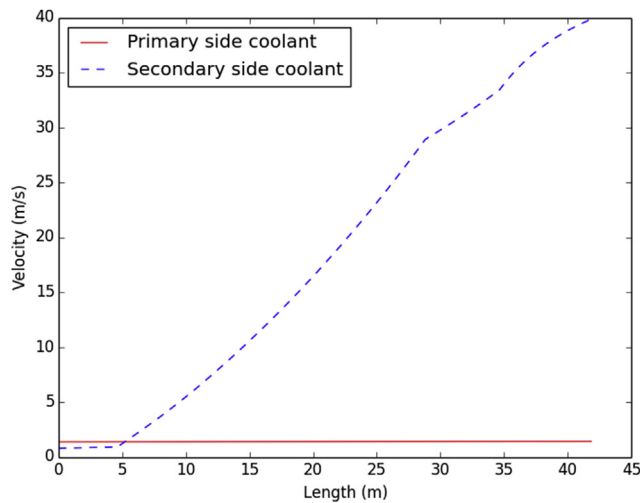**Fig. 4.** Humidity and dryout point of steam generator in MRX. MRX, Marine Reactor X.

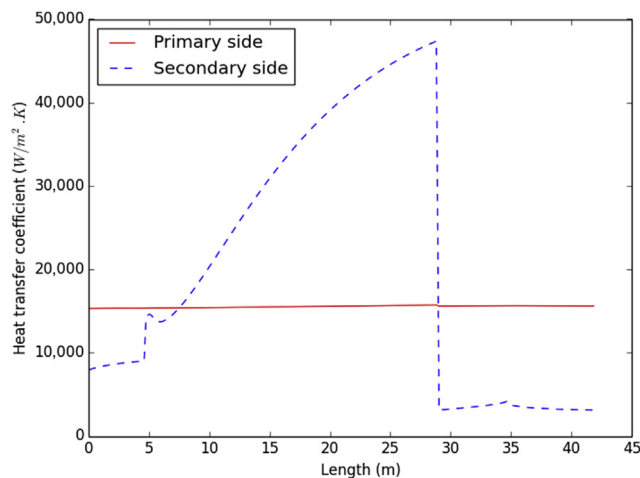**Fig. 5.** Velocity profiles in the MRX steam generator. MRX, Marine Reactor X.

Fig. 6. Heat transfer coefficient profile in the MRX steam generator. MRX, Marine Reactor X.
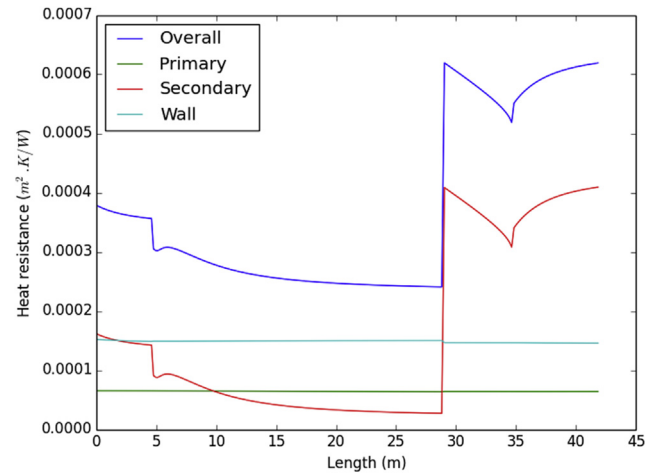

Fig. 7. Heat resistance of steam generator in MRX. MRX, Marine Reactor X.

4. Conclusions

A computer code, THAOT, has been developed for the numerical simulation of an H-OTSG. The code is benchmarked by comparing the design data of the MRX and SMART steam generators. The results calculated by THAOT agree well with the benchmark data. Therefore, THAOT can be used as a thermal−hydraulic tool to analyze an H-OTSG.

However, THAOT has several shortcomings. The heat transfer coefficients and pressure drop are calculated by empirical correlations. Therefore, the predictive accuracy of THAOT is limited by the scope of the empirical correlations. An extensive experimental program, including heat transfer coefficient experiments, pressure drop experiments, and oscillation experiments, has been planned for the improvement of the code.

As China is developing different kinds of small pressurized water reactors that utilize H-OTSG, THAOT can be used to help in thermal−hydraulic design and analysis. Transient analysis of an H-OTSG under development will be presented in the future.

Conflicts of interest

The authors declare that there are no conflicts of interest regarding the publication of this paper.

Acknowledgments

Nomenclature

A	heat transfer area (m^2)
d	inner tube diameter (m)
d_o	outer tube diameter (m)
D	helix diameter (m)
De	Dean number ($-$)
f	friction coefficient ($-$)
f_c	friction coefficient for helical pipe ($-$)
f_s	friction coefficient for straight pipe ($-$)
G	mass flowrate (kg/m^2·s)
h	heat transfer coefficient (W/m^2.K)
L	length (m)

Nu	Nusselt number (−)
P	pressure (Pa)
Pr	Prandtl number
q	heat flux (W/m^2)
r	fouling heat resistance (m^2.K/W)
Re	Reynolds number (-)
u	velocity (m/s)
x	steam quality (−)

Greek symbols

α	Helix angle (°)
ρ	density (kg/m^3)
λ	thermal conductivity (W/m·K)
σ	relative distance (−)
μ	dynamic viscosity (Pa.s)
δ	tube thickness (m)
$\varDelta$	roughness (−)
τ	surface tension (mN/m)

Subscripts

c	cold side
cr	critical
f	liquid phase
fg	phase change
g	gas phase
h	hot side
i	ith control volume
w	wall

References

[1] A.M. Fsadni, J.P.M. Whitty, A review on the two-phase heat transfer characteristics in helically coiled tube heat exchangers, Int. J. Heat Mass Transfer 95 (2016) 551−565.

[2] N.V. Hoffer, P. Sabharwall, N.A. Anderson, Modeling a Helical-coil Steam Generator in RELAP5-3D for the Next Generation Nuclear Plant, Idaho National Laboratory, Idaho Falls, ID, 2011.

[3] J. Yoon, J.-P. Kim, H.-Y. Kim, D.J. Lee, M.H. Chang, Development of a computer code, ONCESG, for the thermal−hydraulic design of a once-through steam generator, J. Nucl. Sci. Technol. 37 (2000) 445−454.

[4] C.P. Tzanos, A movable boundary model for once-through steam generator analysis, Nucl. Technol. 82 (1988) 5−17.

[5] G. Berry, Model of a Once-through Steam Generator with Moving Boundaries and a Variable Number of Nodes, Am. Soc. Mech. Eng. Annu. Mtg., Boston, MA, 1983.

[6] A. Cioncolini, L. Santini, An experimental investigation regarding the laminar to turbulent flow transition in helically coiled pipes, Exp. Therm. Fluid Sci. 30 (2006) 367−380.

[7] S.K. Lee, S.H. Chang, Experimental study of post-dryout with R-134a upward flow in smooth tube and rifled tubes, Int. J. Heat Mass Transfer 51 (2008) 3153−3163.

[8] D. Cao, Thermal−technical Analysis of Once-through Big Helical Tube Steam Generator, Tsinghua University, 2005.

[9] H. Ju, Z. Huang, Y. Xu, B. Duan, Y. Yu, Hydraulic performance of small bending radius helical coil-pipe, J. Nucl. Sci. Technol. 38 (2001) 826−831.

[10] P.V. Gilli, Heat transfer and pressure drop for cross flow through banks of multistart helical tubes with uniform inclinations and uniform longitudinal pitches, Nucl. Sci. Eng. 22 (1965) 298−314.

[11] Office of Nuclear Ship Research and Development, Conceptual Design of the Advanced Marine Reactor MRX, JAERI-M 91−9004, 1991.

[12] T. Ishida, Advanced Marine Reactor MRX and its Application for Electricity and Heat Co-generation, Small Power and Heat Generation Systems on the Basis of Propulsion and Innovative Reactor Technologies, IAEA-TECDOC-1172, Vienna, 2000.